

Numerical Modeling of Transient Basin and Range Extensional Geothermal Systems

J. R. McKenna and D. D. Blackwell

Southern Methodist University
Department of Geological Sciences
3225 Daniel Street
Dallas, Texas, 75275, USA
email: jmckenna@mail.smu.edu
email: blackwel@passion.isem.smu.edu

ABSTRACT

A suite of models utilizing a range of bulk rock permeabilities were developed to analyze the transient behavior of basin and range extensional geothermal systems, and particularly, the evolution of the system temperature with time. Each model consists of two mountain ranges (~1 km relief from the valley floor) separated by a thick sequence (about 4 km) of clastic sediments derived from the adjacent ranges, and a relatively permeable, high angle fault that functions as a conduit for subsurface fluids. This geometry is typical of Basin and Range extensional systems.

We characterize the reservoir by utilizing several parameters, including temperature along the producing fault, maximum temperature away from the fault in the probable reservoir region, and finally, the predicted surface heat flow.

INTRODUCTION

Active geothermal systems in which subsurface temperatures are sometimes in excess of 200 °C, and even 250 °C by 2-3 km depth, are often associated with Quaternary normal faulting in the Basin and Range. These systems are non-magmatic in origin. Meteoric water enters via the range top or valley fill, warms during deep circulation, and ascends along the nearest permeable pathway, usually an active range-bounding fault. One such Basin and Range geothermal system located in Dixie Valley, Nevada is unusually hot: temperatures in excess of 280 °C have been encountered by 3 km depth.

Our objective in this study is to determine under what conditions a reservoir temperature near 280 °C is generated and if possible, sustained. We characterize the reservoir by utilizing several parameters, including temperature along the producing fault, maximum temperature away from the fault in the probable reservoir region, and finally, the predicted surface heat flow.

Figure 1 is a shaded relief map Dixie Valley, Nevada, and the adjacent region. Several hot springs and fumaroles are located within the valley indicating high subsurface temperatures.

The models we present are similar to the natural geometry of extensional geothermal systems: two mountain ranges (~1 km relief from the valley

floor) separated by a thick sequence (about 4 km) of clastic sediments derived from the adjacent ranges, and a relatively permeable, high angle fault (65°) that functions as a conduit for subsurface fluids.

Recent attempts to characterize the flow regime in these types of systems Wisian (2000) utilizing TOUGH2 (Pruess et al., 1999) have concentrated on exploring the parameter space of the numerical models necessary to establish sufficient upflow along a permeable fault to match 1) the observed discharge at the fault/valley contact, and 2) the steady-state temperature distribution.

Here, we describe the transient results of our numerical modeling to illustrate the complexity inherent in these systems, and as a explanation potential for reconciling higher observed reservoir temperatures (from precision temperature logs) than predicted by steady-state models.

STEADY-STATE RESULTS

Model Geometry

The geometry utilized in the numerical modeling is illustrated in Figure 2. The modeling parameters specific to each numbered domain are listed in Table 1. Note that the valley fill incorporates anisotropic permeability to minimize the discharge in the valley in accord with observations. The cell size away from the fault zone is 230 m x 90 m, whereas immediately adjacent to the fault, the cell size is halved. (130 m x 45 m) to provide sufficient resolution of both the thermal and flow regime near the fault. The total number of elements is 7837.

The models shown here were all developed utilizing PetraSim by Thunderhead Engineering Consultants. Unless stated otherwise, all the models developed in this study utilize surface temperature and pressure boundary conditions of 20 °C, and 1×10^5 Pa, respectively. Additionally, a basal heat flow of 90 mWm^{-2} directed into the model (chosen so that the model accurately represents the high heat flow Basin and Range Province) is specified for the bottommost row of cells.

We utilize a modified version of the equation-of-state for pure water (EOS1) for TOUGH2 that allows for super-critical conditions in pure water (EOS1sc; Brikowski, 2001). Both the

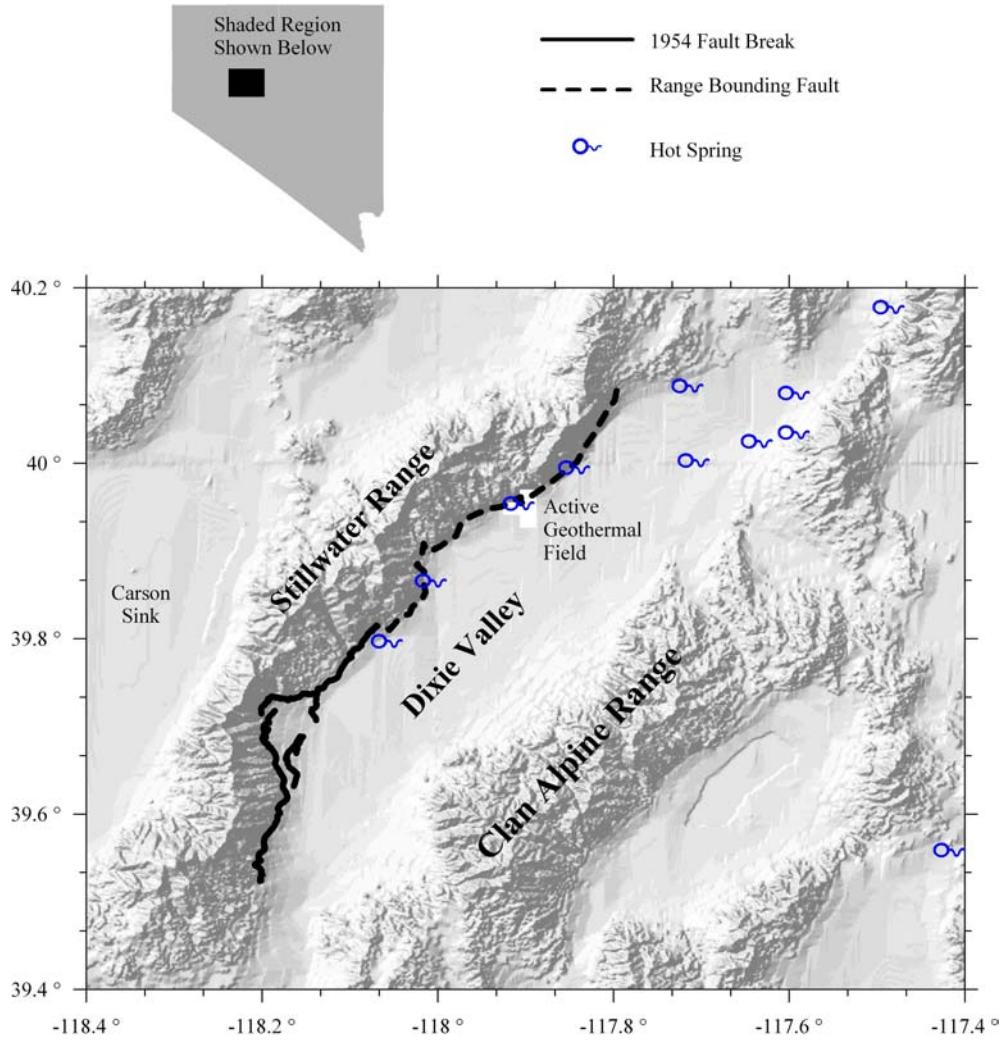


Figure 1. Dixie Valley, Nevada. All subsequent numerical models attempt to model the “active geothermal area”.

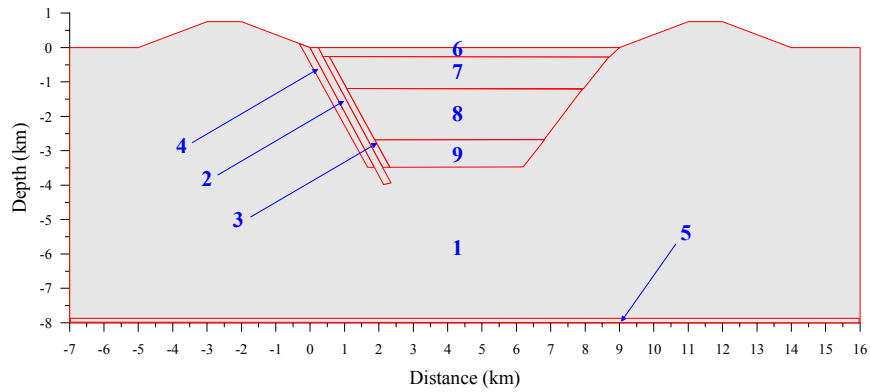


Figure 2. Model geometry. The domain number in the above figure corresponds with the domain number appearing in Table 1.

EOS1 and EOS1sc modules yield almost identical results; however, because even non-magmatic geothermal systems are often near the critical point of pure water by 6-9 km depth, the latter module provides more realistic characterization of reservoir pressure-temperature conditions. Also to facilitate direct comparison with future models with higher temperatures, we use the super-critical equation-of-state module.

Thermal and Flow Regime

Figure 3 shows the steady-state temperature and velocity distribution obtained after a simulation time of 32 Myr (hereafter referred to as steady-state) utilizing a bulk rock permeability of $1 \times 10^{-20} \text{ m}^2$ (i.e., domain 1, see Figure 2). Refer to the Figure caption for details. At such a low permeability, almost all the fluid velocities are low (with the exception of the range tops), and the only observed thermal effect is a modest increase in temperature between the ranges (domains 6-9 in Figure 2) due to the low thermal conductivity valley fill. Both the linearity of the temperature along the fault as a function of depth (Figure 4; see below) and the lack of anomalously high predicted surface heat flow at the fault/range contact (Figure 5) illustrate that the model is essentially conductive.

Because most geothermal systems are believed to thermally evolve from a conductive regime as the range-bounding fault permeability abruptly increases during/after an earthquake, the steady-state temperature and pressure (not shown) conditions obtained from the model shown in Figure 3 are utilized as the initial conditions for all subsequent models.

We restrict the subsequent analysis to two values for the bulk rock permeability: 1×10^{-16} and $5 \times 10^{-16} \text{ m}^2$, for two reasons. First, at bulk rock permeabilities $> 1 \times 10^{-16} \text{ m}^2$, models do not attain steady-state. In fact, the models progress in almost real-time: one day of computational time with a Pentium IV 2.4 GHz processor results in a simulation time of only 1 week. Second, at permeabilities lower than $1 \times 10^{-16} \text{ m}^2$ models are essentially conductive: a model utilizing a bulk rock permeability of $1 \times 10^{-17} \text{ m}^2$ generates fault temperatures that are $< 2 \text{ }^\circ\text{C}$ different from the conductive model (i.e., $1 \times 10^{-20} \text{ m}^2$, see Figure 4).

The steady state results for bulk permeabilities of 1×10^{-16} and $5 \times 10^{-16} \text{ m}^2$ are shown in Figures 6 and 7, respectively. In both cases recharge occurs in the ranges, whereas discharge occurs at the fault/valley fill contact. Furthermore because the fault serves as a conduit for the upflow of fluids, temperatures along the fault are at least $125 \text{ }^\circ\text{C}$ hotter than at the other side of the valley fill-range contact (Figures 6 and 7).

Other than the qualitative similarities noted above, the thermal and flow regimes between the two

permeabilities are quite different. The higher permeability case has significantly more fluid flow up the fault, partly because the greater permeability contrast between the anisotropic valley fill and bulk rock focuses recharge from the adjacent ranges into the valley-fill sequence, and partly because the $\sim 5 \text{ km}$ diameter secondary convection cells that have developed beneath the ranges help deliver more fluid to the fault inlet area. Hence the flow field for the higher permeability case ($5 \times 10^{-16} \text{ m}^2$) is almost a factor of 2 faster than in the lower permeability case ($1 \times 10^{-16} \text{ m}^2$). It is noted that a correspondingly greater recharge rate in the ranges is predicted to account for the large amount of fluid discharging at the fault/valley fill contact. The models presented here predict a maximum steady-state discharge at the fault/valley contact of about $17,000 \text{ ltyr}^{-1}$ ($1 \times 10^{-16} \text{ m}^2$ case) and about $45,000 \text{ ltyr}^{-1}$ ($5 \times 10^{-16} \text{ m}^2$ case). We calculate the discharge in the Dixie Valley area to be about $31,600 \text{ ltyr}^{-1}$. Hence the models shown here predict similar volumetric flow rates.

In summary, the less vigorous flow regime for the lower bulk rock permeability model lacks the secondary convection observed for the higher bulk rock permeability model probably because the flow is focused along the model boundaries. Future models will expand the dimensions of the model to determine if the lack of secondary convection beneath the ranges for lower permeability bulk rock is a meaningful result, or is simply a case of the model boundaries imposing the observed flow regime.

Surface Heat Flow

The steady-state predicted surface heat flow for the conductive (a bulk rock permeability of $1 \times 10^{-20} \text{ m}^2$) and non-conductive models (bulk rock permeabilities of 5×10^{-16} and $1 \times 10^{-16} \text{ m}^2$) are illustrated in the upper panel of Figure 5. In the conductive case, the predicted heat flow is approximately equal to the basal heat flow, although the overall shape of the curve is complicated by heat refraction effects from the dipping fault/valley fill contact. The non-conductive models show a $> 450 \text{ mWm}^{-2}$ heat flow anomaly centered on the fault/valley fill contact. Additionally, the $1 \times 10^{-16} \text{ m}^2$ model predicts a heat flow anomaly about 100 mWm^{-2} greater than the $5 \times 10^{-16} \text{ m}^2$ bulk rock permeability model due to the higher fluid recharge rate in the ranges.

Fault Temperature

The fault temperature for the steady-state thermal regimes modeled in Figures 3, 6, and 7 appear in Figure 4 along with the conductive solutions discussed previously. In each case, the temperature is extracted along the fault (the solid line dipping at 65° in each thermal cross-section) and

Table 1. TOUGH2 modeling parameters. A constant density and heat capacity of 2650 kgm^{-3} , and $1000 \text{ Jkg}^{-1}\text{K}^{-1}$, respectively were utilized in the modeling. The Bulk Rock permeability is varied in each model. Unless noted otherwise, a basal heat flow of 90 mWm^{-2} , surface temperature of $20 \text{ }^\circ\text{C}$, and surface pressure of $1.01 \times 10^5 \text{ Pa}$ were specified as boundary conditions.

Domain	Material	Porosity	Wet Thermal Conductivity ($\text{Wm}^{-1}\text{K}^{-1}$)	Horizontal Permeability (m^2)	Vertical Permeability (m^2)
1	Bulk Rock	1.0E-01	2.50	Variable	Variable
2	Fault	1.0E-01	2.50	1.0E-14	1.0E-14
3	Fault, Right-Side	1.0E-01	1.25	1.0E-18	1.0E-18
4	Fault, Left-side	1.0E-01	2.50	1.0E-18	1.0E-18
5	Bottom	1.0E-05	2.50	1.0E-20	1.0E-20
6	Valley-Fill 1	1.0E-01	1.25	1.0E-15	1.0E-16
7	Valley-Fill 2	1.0E-01	1.25	1.0E-15	1.0E-16
8	Valley-Fill 3	1.0E-01	1.25	1.0E-15	1.0E-16
9	Valley-Fill 4	1.0E-01	1.25	1.0E-15	1.0E-16

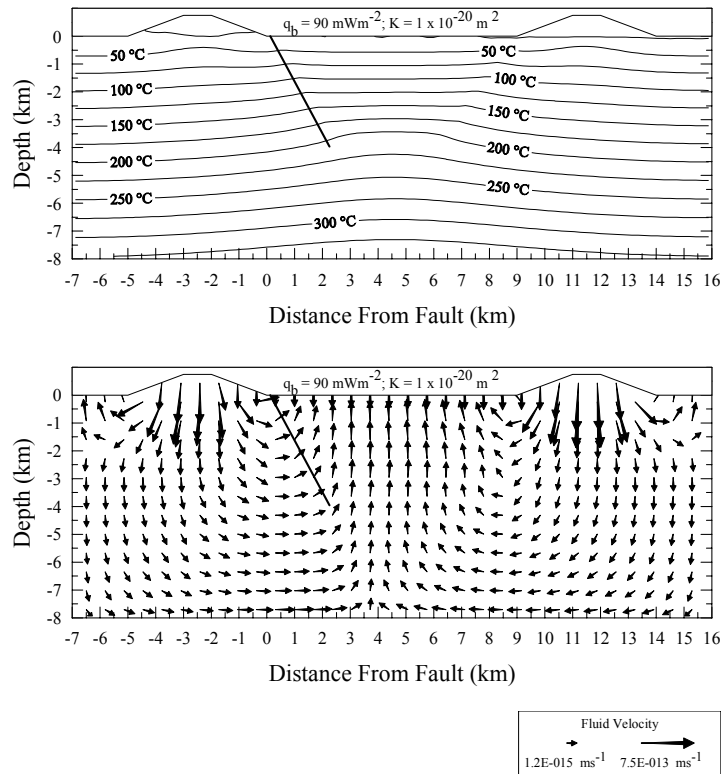


Figure 3. Steady-state thermal and flow regime obtained utilizing a bulk rock permeability of $1 \times 10^{-20} \text{ m}^2$, and a basal heat flow of 90 mWm^{-2} . The permeable fault is shown as a heavy solid line. The thermal regime is essentially conductive.

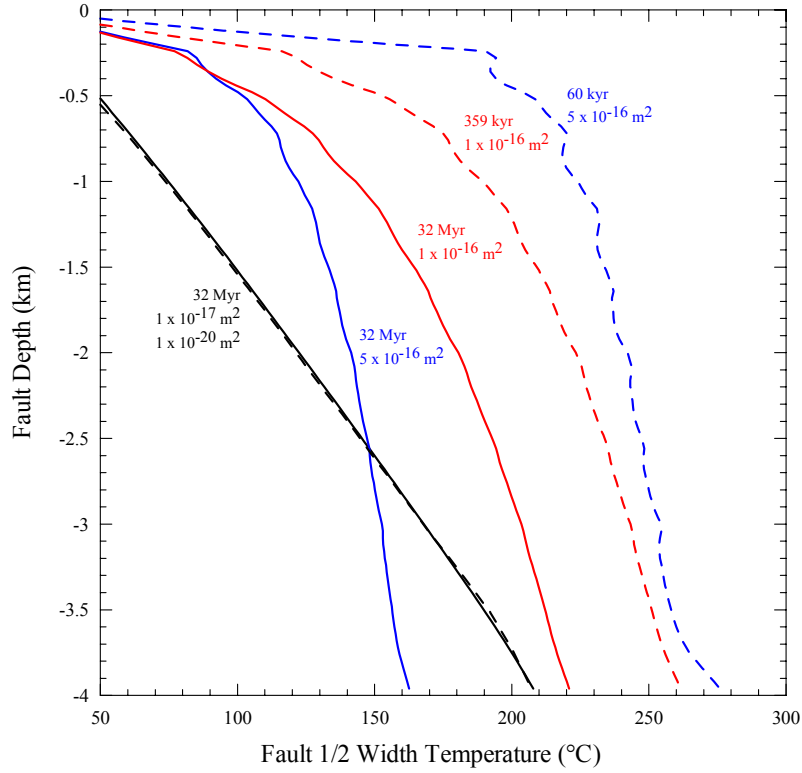


Figure 4. Predicted fault temperature for several bulk rock permeabilities and simulation times.

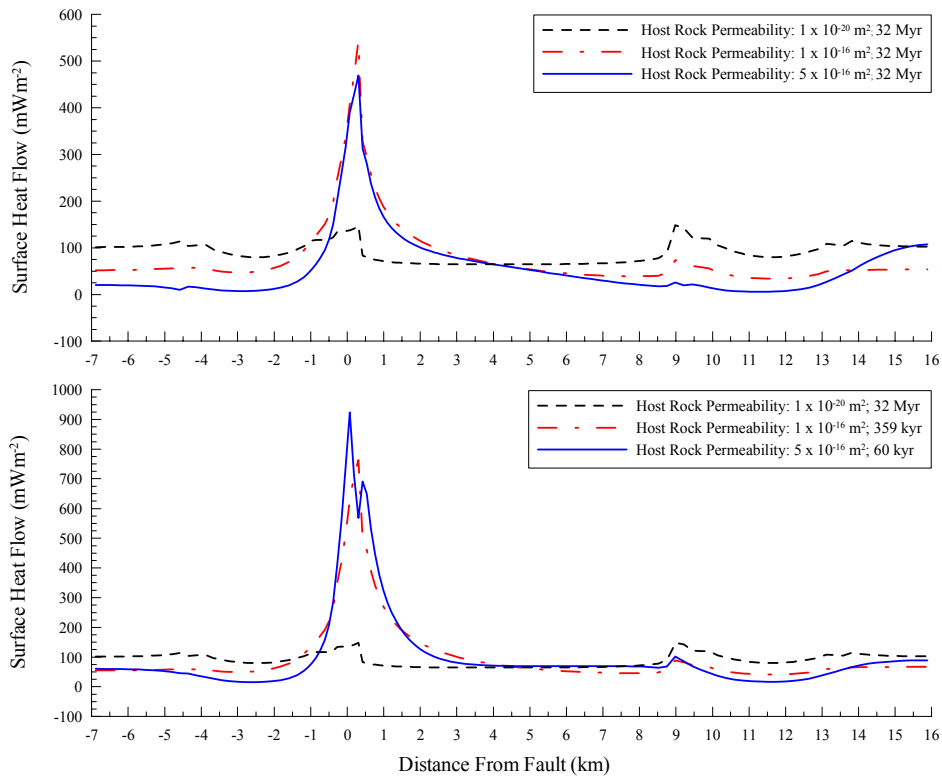


Figure 5. Predicted surface heat flow at 0 km depth for several bulk rock permeabilities and simulation times.

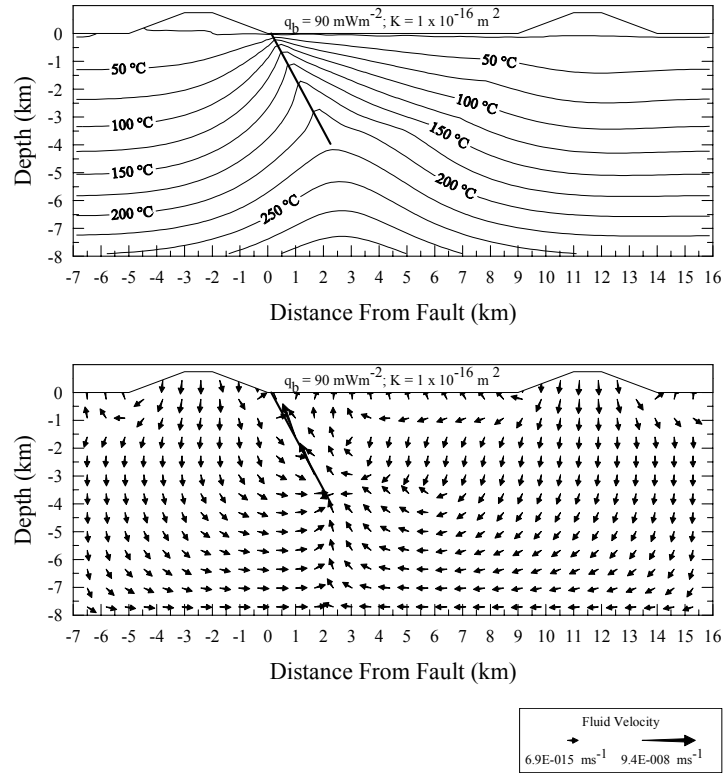


Figure 6. Steady-state thermal and flow regime obtained utilizing a bulk rock permeability of $1 \times 10^{-16} \text{ m}^2$, and a basal heat flow of 90 mWm^{-2} .

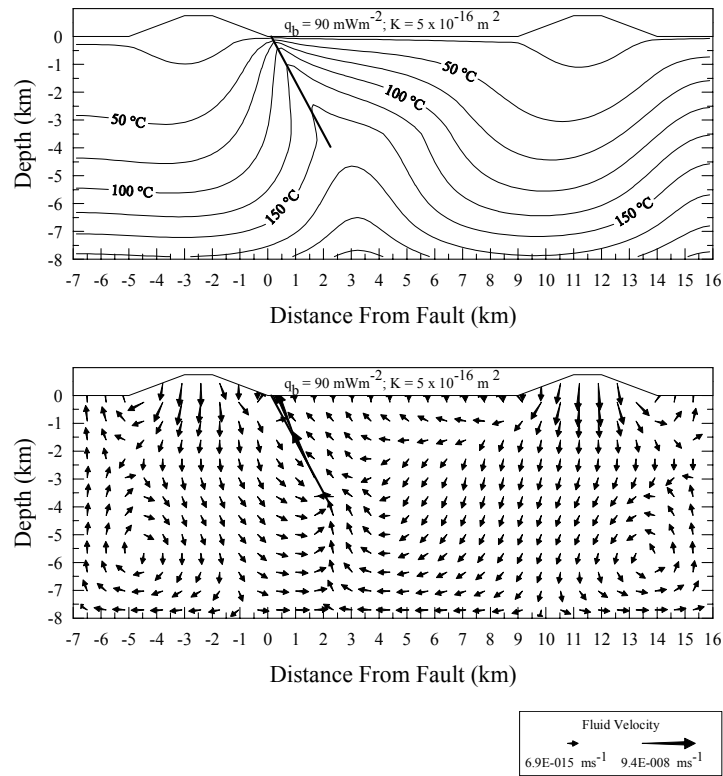


Figure 7. Steady-state thermal and flow regime obtained utilizing a bulk rock permeability of $5 \times 10^{-16} \text{ m}^2$, and a basal heat flow of 90 mWm^{-2} .

plotted as a normal function of depth. The maximum steady-state fault temperature is about 220 °C for the lower bulk rock permeability model and about 160 °C for the higher bulk rock permeability model. These temperatures are significantly lower than the ~280 °C temperatures measured via precision temperature logs in Dixie Valley, and in the case on the higher bulk rock permeability model, extremely low (about 120 °C lower). The shape of the temperature-depth curves offers one possible explanation.

In typical extensional geothermal systems the fault temperature at shallow depths (0-3 km) is significantly warmer than a purely conductive model at an identical depth. However, even with modest upflow, the fault should remain at least as warm as the conductive model over the entire fault depth. The severe departure of the $5 \times 10^{-16} \text{ m}^2$ bulk rock permeability model from this ideal suggests that transient effects may be important in this particular model, and regional flow models in general.

TRANSIENT RESULTS

Geothermal systems may require periodic earthquakes to prevent self-sealing of the permeable fault, hence the maximum fault temperature should tract the recurrence interval on the fault. Typical Basin and Range faults appear to sustain large earthquakes every 1-20,000 years. The southern Dixie Valley fault last ruptured in 1954, but the area where the geothermal system is located has not ruptured for several thousand years (J. Caskey, personal communication, 2002). The problem of reconciling higher observed reservoir temperatures (from precision temperature logs) with the lower temperatures modeled at steady-state, thus becomes the problem of determining where in the temporal-evolution of the geothermal system production is situated. Hence in we next assess the effects of transient heating and cooling in the models developed above.

Fault Temperature

Figure 8 are the temperature-time histories for a cell located at the downdip edge of the fault, approximately 3.85 km below and 2.15 km to the right of the fault/valley contact (see Figure 2) utilizing several bulk rock permeabilities. The cell therefore records the maximum fault modeled temperature. For models utilizing bulk rock permeabilities of $1 \times 10^{-17} \text{ m}^2$ or below, the thermal regime is essentially conductive, and the temperature quickly reaches steady-state with only a few degrees of heating. For the higher bulk rock permeabilities, however, the temperature at the base of the fault varies strongly as a function of time. The maximum temperature for these cases is 255-275 °C and does not occur at steady-state, but rather, within the first

60 kyr for the $5 \times 10^{-16} \text{ m}^2$ bulk rock model, and 359 kyr for the $1 \times 10^{-16} \text{ m}^2$ bulk rock model.

We believe that a time step of 0.6-2.5 kyr used by TOUGH2 at simulation times < 1 Myr is sufficient to resolve the transient behavior. Thus, it appears that the much like actual geothermal systems, the models presented here “mine” heat over time causing the system to cool significantly. Thus the large difference between the steady-state temperatures predicted by the 1×10^{-16} and $5 \times 10^{-16} \text{ m}^2$ models can be explained by the secondary convection present beneath the ranges in the one model mining not only more heat, but at a faster rate. So much so, that the overall thermal regime is cooler. The secondary convection that develops as the system evolves may however be influenced by the model geometry. Future work will expand the distance between the ranges, as well as deepen the model to > 10 km depth to investigate this effect.

Because both bulk rock permeability models predict temperatures that are lower than the ~ 280 °C temperatures measured via precision temperature logs in Dixie Valley, several models were created to test the effect of a deepening the fault and valley fill by 2 km. Figure 8 also shows the results from these models. Again, each temperature-time history is well-resolved, however the maximum temperature for the lower bulk rock permeability case occurs at about 200 kyr earlier, whereas the maximum temperature for the higher bulk rock permeability case occurs about 20 kyr later. The increase in fault temperature raises is only about 10-15 °C, which albeit a small increase, is sufficient to match the measured temperature.

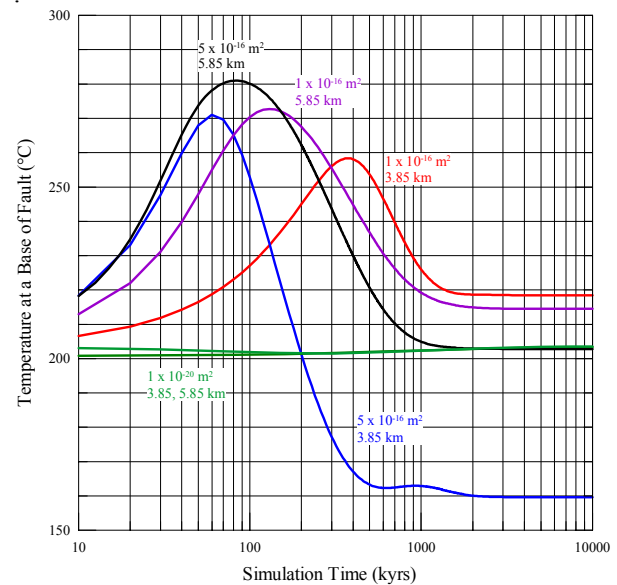


Figure 8. Temperature-time history of a cell at the base of the fault (either 3.85 or 5.85 km) for several bulk rock permeabilities.

Surface Heat Flow

The predicted surface heat flow for the models at the simulation time corresponding to the maximum fault temperature for three different bulk rock permeability models (1×10^{-20} , 1×10^{-16} , and $5 \times 10^{-16} \text{ m}^2$) are shown in the lower panel of Figure 5 (note the vertical scale change between the two panels). Because the maximum fault temperature for the conductive case occurs at steady-state, the predicted heat flow does not change. However the predicted heat flow at the fault/valley contact is almost 200 mWm^{-2} ($1 \times 10^{-16} \text{ m}^2$ case) and 500 mWm^{-2} ($5 \times 10^{-16} \text{ m}^2$ case) higher than for their respective steady-state cases. Furthermore, the predicted range heat flow is somewhat higher due to the lower recharge rates at the earlier simulation times. Also note that the double peak in the predicted heat flow near the fault/valley contact for the ($5 \times 10^{-16} \text{ m}^2$ bulk rock permeability case) is an artifact of the manner in which the heat flow is calculated and is therefore not meaningful.

Wisian et al (2001) calculated a heat loss of $1 \times 10^7 \text{ W}$ for the Dixie Valley geothermal system. Normalizing their results by the actual geothermal production area (12 km^2 ; 6 km along strike \times 2 km along dip), the Dixie Valley heat loss is about 833 mWm^{-2} . Clearly, the best match to the observed heat loss is obtained from the models incorporating a bulk rock of $5 \times 10^{-16} \text{ m}^2$ at 60 kyr , and 359 kyr for a bulk rock at $1 \times 10^{-16} \text{ m}^2$.

CONCLUSIONS

The most important observations obtained from our simulations are that transient effects in these types of systems can dramatically modify the maximum predicted reservoir temperature. For example, the maximum fault temperature of about $275 \text{ }^\circ\text{C}$ obtained utilizing a bulk rock permeability of $5 \times 10^{-16} \text{ m}^2$ does not occur at steady-state, but rather at 60 kyr , and is about $110 \text{ }^\circ\text{C}$ hotter than at steady-state. The $1 \times 10^{-16} \text{ m}^2$ bulk rock permeability model behaves similarly. It is interesting to note that a 2 km deeper fault yields similar behavior and temperatures. Furthermore, because the deeper fault models (and shallower fault models) satisfy the observed fault temperature, flow rates, and heat flow, we believe that high permeability persists to at least 6 km depths.

The complicated flow regimes modeled suggest that the heat present in the system is “mined” over time causing the system to cool significantly, but nonetheless, the system persists for millions of years at commercially exploitable temperatures. Hence, the problem of reconciling higher observed reservoir temperatures (from precision temperature logs) with the lower temperatures modeled at steady-state, becomes the problem of determining where in the temporal-evolution of the geothermal system production is situated. If higher temperatures are required, they are easily obtained from the models

simply by assuming that the present thermal and flow regime is early in the system’s cycle. In fact, the present day heat loss from the Dixie Valley geothermal system suggest that the system is not at steady-state, but rather somewhat earlier in the temporal evolution, perhaps only a few hundred thousand years.

However, some process must still prevent the system from mining enough of the heat so that it “shuts-off” completely. The relatively high reservoir temperatures commonly observed in geothermal systems ($> 280 \text{ }^\circ\text{C}$) must be a function of oscillating high/low fault permeability maintained by seismicity along the range-bounding fault. Thus, the geothermal fluid is never truly depleted: the upflow simply wanes with decreasing fault permeability, and perhaps is rerouted elsewhere.

Regardless, the transient nature of the systems modeled suggest a much more complex situation than previously thought, but provide a reasonable explanation to the high observed fault temperatures.

ACKNOWLEDGMENTS

This work was supported by D.O.E. Contract DE-FG07-02ID14414 to D.D.B. The authors wish to acknowledge Ken Wisian for help setting up the models.

REFERENCES

- Blackwell, D.D., M. Leidig, and R.P. Smith, Regional Geophysics of the Dixie Valley Area: Example of a Large Basin and Range Geothermal System, *Geotherm. Resour. Council Trans.*, pp. 519-523, 2002.
- Brikowski, T. H., Modeling Supercritical Systems With TOUGH2: The EOS1sc Equation of State Module and a Basin and Range Example, *Geotherm. Resour. Council Trans.*, pp. 285-290, 2001
- Pruess, K., C. Oldenburg, and G. Moridis, *TOUGH2 User’s Guide, Version 2.0*, Report LBNL-43134, Lawrence Berkeley National Laboratory, Berkeley, Calif., 1999.
- Wisian, K. W., Insights into Extensional Geothermal Systems from Numerical Modeling. *Geotherm. Resour. Council Trans.*, pp. 281-286, 2000.
- Wisian, K. W., D.D. Blackwell, and M. Richards, Correlation of Surface Heat Loss and Total Energy Production for Geothermal Systems. *Geotherm. Resour. Council Trans.*, pp. 331-336, 2001.